NUKLEONIKA 2002;47(4):147–150

ORIGINAL PAPER

Studies of plasma and craters produced by the interaction of high-energy sub-nanosecond laser with silver target

Eugeniusz Woryna, Jan Badziak, Piotr Parys, Romana Suchańska, Jerzy Wołowski, Josef Krása, Leoš Láska, Miroslav Pfeifer, Karel Rohlena, Jiři Ullschmied

Abstract The results of measurements of microablation from a silver target irradiated by the high-power PALS laser system in Prague are presented. In this experiment the laser beam of energy of about 110 J in a 400 ps pulse was focused perpendicularly to the massive silver target. The target surface position was changed with respect to the focal spot of the laser beam in the range from -2.5 to 2.5 mm. A set of four ion collectors was used for plasma ion emission measurements. The effect of the laser pulse interaction with the target, i.e. craters and damages formed in the vicinity of the craters, were investigated with the use of scanning electron microscopy (SEM) and optical microscopy methods. The characteristics of the crater were compared with the essential parameters of ion streams emitted from the plasma produced in the same laser shot.

Key words ion beam • laser • laser-induced crater • plasma

E. Woryna✉, J. Badziak, P. Parys, R. Suchańska, J. Wołowski
Institute of Plasma Physics and Laser Microfusion,
23 Hery Str., P.O. Box 49, 00-908 Warsaw, Poland,
Tel.: +48 22/ 683 96 05, Fax: +48 22/ 666 83 72
e-mail: woryna@ifpilm.waw.pl

J. Krása, L. Láska, M. Pfeifer, K. Rohlena, J. Ullschmied
Institute of Physics,
Academy of Sciences of the Czech Republic,
2 Na Slovance Str., 182 21 Prague, Czech Republic

Received: 24 October 2001, Accepted: 28 June 2002

Introduction

The interaction of high-power laser pulses with solids (metals, semiconductors, dielectrics and organic materials) has been studied since the early stages of laser development [11]. There was and still is a great deal of interest in utilizing laser ablation and crater formation for practical applications. However, the ablation mechanism and cratering processes are strongly depended on both the laser pulse parameters and the material properties. These mechanisms for ultrashort (femto- and picosecond) laser pulses [12, 14, 16] differ significantly from that for nanosecond pulses [1–3, 9, 10, 15]. The laser energy density on the target for ultrashort laser pulses is very low (usually below 10 J/cm^2) whereas for nanosecond pulses it reaches values of several 10^6 J/cm^2. Focusing a beam of a high-power nanosecond pulse laser onto a solid target causes that a considerable part of the beam energy and momentum is transferred to the target. The rapid heating of surface material yields a high pressure of the order of megabars. As a result, a shock wave is generated with typical velocity up to several km/s. In these conditions a violent evaporation of the target material follows and in the place where laser radiation is impinging, a crater appears. Its dimension depends on the laser beam parameters (the laser intensity, the focused spot size, the laser pulse duration) as well as on the physical properties of the target material. A shock wave passing completely through the target is followed by a rarefaction wave moving into the compressed material behind the original shock wave. On the rear of the target surface a bulge appears.

Energy and velocity distribution of ions emitted from a plasma after relativistic self-focusing were investigated theoretically and compared with experimental results [6].

The aim of this experiment was to investigate the crater shapes and the expanding plasma stream and to find correlations between them.

Experimental set-up

The high power iodine photodissociation Prague Asterix Laser System (PALS) [7] delivering up to 700 J of energy in 0.4 ns at the wavelength of 1.315 μm was used in the experiment. The laser beam was focused perpendicular to a massive 1 mm thick silver target with the use of an aspherical lens. According to the lens certificate, the focal length and the focus spot diameter for λ=1.315 μm was 593 mm and 70 μm, respectively. The lens has a ∅30 mm hole in the centre to prevent the destruction by the part of the laser beam reflected and focused by the inner lens surfaces. This hole was screened off by a mask of 35 mm in diameter. The target surface position was changed with respect to the distance of the focal spot of the laser beam within the range from FP=-2.5 mm to FP=2.5 mm. The sign "-" means that the focal spot was in front of the target surface, sign "+" – the focal spot was inside the target volume. The FP=0 means that the target surface is in the in-focus position (position of the geometrical laser focus). Four ion collectors (ICs) placed at distances of 42, 59, 51 and 46 cm from the target and at angles of 23, 37, 52 and 62° with respect to the laser beam axis, respectively, and an electrostatic ion energy analyzer (IEA) placed at a distance of 287 cm at an angle of 30° with respect to the laser beam axis were used to investigate the effect of the focusing conditions on the characteristics of the emitted ion streams [13]. The ICs deliver time-resolved signals of ion current from which the total charge carried by ions and the average ion energy can be calculated. The IEA gives the possibility of identifying the ion species produced, i.e. determining their charge-to-mass ratio, energy and abundance on the basis of ion spectra recorded for different analyzing voltages. The background pressure in the experimental chamber was 2.6×10^{-6} mbar.

Experimental results

Results of plasma investigation

Four ion collectors used in the experiments provided information on the angular behavior of the expanding plasma stream. Over the whole range of focusing conditions the angular distribution of the charge carried by the ions fulfils the dependence

(1) $$Q = Q_0 \cos^x\alpha,$$

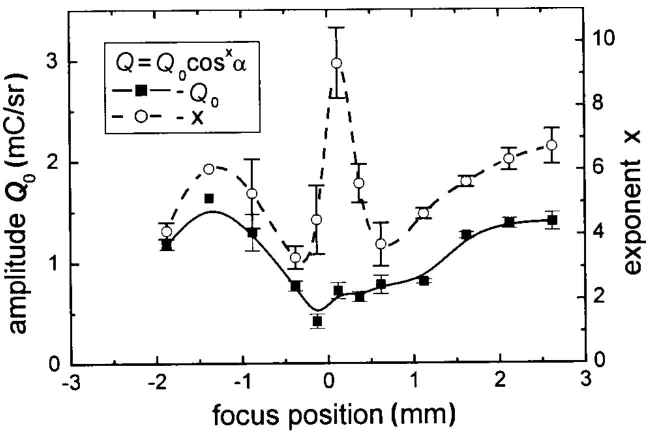

Fig. 1. The amplitude Q_0 and exponent x of the angular distribution of silver ions.

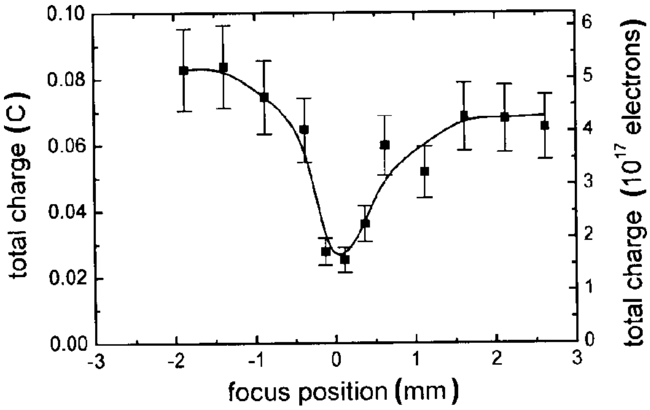

Fig. 2. The total charge carried by silver ions.

where Q_0 is the charge carried in normal direction to the target surface and x is the exponent of the power function. Q_0 and x take extremal values around FP=0 (Fig. 1).

The dependence of the total charge carried by the ions

(2) $$Q_{tot} = 2\pi Q_0 \int \cos^x\alpha \cdot \sin\alpha \cdot d\alpha$$

and the maximum ion current density as a function of the focus position are shown in Figs. 2 and 3, respectively. These parameters attain a minimum at the in-focus position on the target surface FP≈0.

The electron temperature, T_{e0}, and the mean charge state of ions, $<z_0>$, in the hot plasma region were estimated using the Busquet formula [4] and the dependence on the average ion energy, $<E_i>$, on T_{e0} and $<z_0>$ in the form $<E_i>= C(<z_0>+1)T_{e0}$. For $<E_i>$=500 keV determined in our experiment and C=4, they were calculated to be $T_{e0}\approx3$ keV and $<z_0>\approx40$. The maximum charge state of Ag ions measured with the use of the IEA was z_{max}=39. Let us try to estimate the laser-induced ablation pressure. The sound velocity of Ag ions is $c_s=(<z_0>T_{e0}/M_i)^{0.5}=3.3\times10^7$ cm/s and the ablation pressure is $p_{abl}\approx2\rho_{cr}c_s^2$=5.6 Mbar (where $\rho_{cr}=n_{ec}(M_i/<z_0>)$=2.6 mg/cm^3 is the critical density of Ag plasma, $n_{ec}=1.12\times10^{21}/\lambda^2= 6.45\times10^{20}$ cm^{-3} is the critical electron concentration for λ=1.315 μm and M_i is the atomic mass of Ag). The value of the ablation pressure is in good agreement with the result presented in [5].

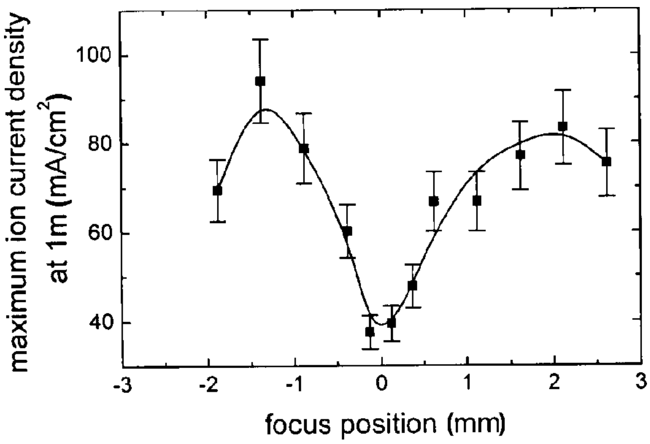

Fig. 3. The maximum ion current density at the distance of 1 m from the target.

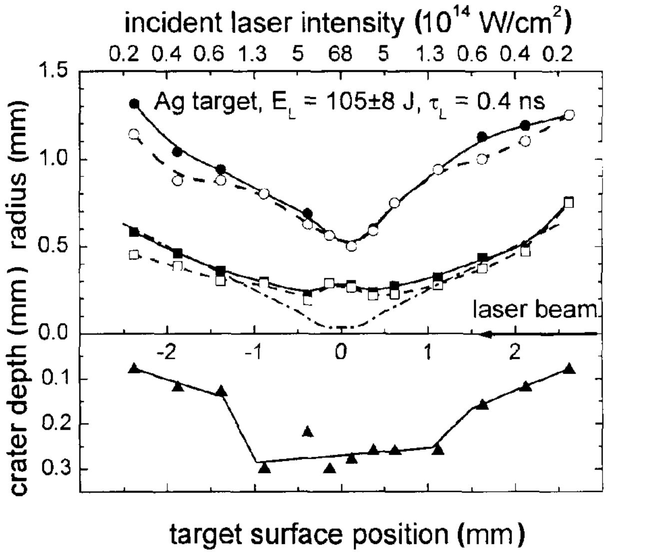

Fig. 4. The radii of craters (■, □ – maximum and minimum radius of crater), damages (•, o – maximum and minimum radius of damages), depth of crater (▲– depth of craters) and the caustic of focusing lens (- · · · – caustic of the focusing lens) as a function of the target surface position.

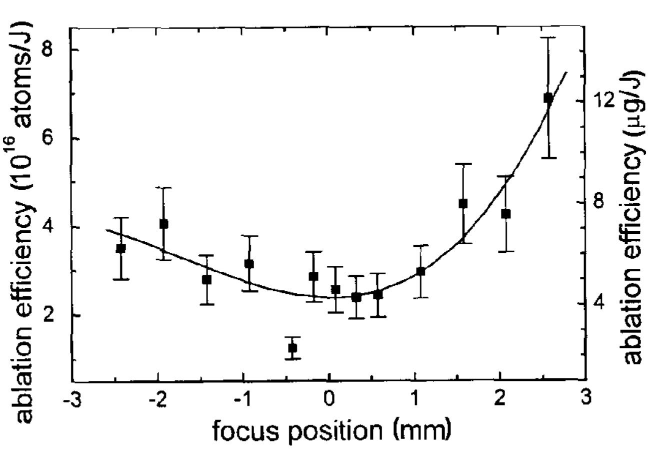

Fig. 5. The ablation efficiency of silver.

Results on crater investigation

The crater dimensions and profiles were deduced on the basis of optical and SEM measurements of craters as well as on their replicas made from acetate cellulose. Figure 4 shows the dependence of the dimensions of the craters and of the target surface damages surrounding the craters (maximum and minimum radii of the craters and of the damages) and the theoretical caustic of the focused laser beam with the waist of 70/280 μm in diameter/length on the focusing conditions present in our experiments for 105±8 J/0.4 ns laser pulses. This means that the maximum laser intensity is $I=6.8\times10^{15}$ W/cm^2 (maximum energy density of 2.7 MJ/cm^2) at FP=0. It is seen that the craters and the damages are non-circular in shape and that the eccentricity is much higher for the defocused laser beam. The crater radius is mainly determined by the laser beam diameter for FP>1.4 mm and FP< -1.4 mm. For -1.4 mm ≤ FP ≤ 1.4 mm the crater radius is much higher (about 8 times) than the radius of the waist and approaches a local maximum around FP≈0. Only for -0.4 mm < FP < 0.4 mm a convexity (a collar) surrounding the crater appears. In general, the crater profiles are asymmetrical relative to FP=0, probably, due to different spatial distribution of laser energy densities at different FP. The value of the crater diameters for FP≈0 are consistent with that shown in [2, 10].

The depth of the craters shows a weak dependence on FP for FP< -1.4 mm and FP>1.4 mm but for -1 mm < FP ≤ 1 mm the crater depth abruptly increases and takes nearly a constant value of about 0.27±0.01 mm. In all laser shots a bulge on the rear side of the target occurs.

The rough estimation of the ablation efficiency, (i.e. mass of the target material ejected from the target) on the basis of the crater volume gives the following values: for FP=-2.5 mm – 6.9 μg/J (3.9×10^{16} atoms/J), for FP=0 – 4.3 μg/J (2.4×10^{16} atoms/J) and for FP=+2.5 mm – 11.6 μg/J (6.3×10^{16} atoms/J). The plot of the ablation efficiency in dependence on the focus position is shown in Fig. 5. This dependence takes a minimum around FP≈0 similar as dependence of the total charge carried by the plasma and the ion current density presented in Figs. 2 and 3. The crater volume and the mass ejected from it at FP=0 agree with the values given in [2, 10].

The structure of damages surrounding the craters, i.e., the radial streams of solidified metal on the target surface suggests that a large area surrounding the crater is in the liquid state during the plasma expansion. Probable reasons of the surface melting may be the following: a quality of the laser beam (far-field diffraction pattern), lateral heat transport or secondary absorption of the X-rays from the plasma volume [8].

Taking into account the results presented in Figs. 2 and 5, the ionization degree of the plasma, i.e. the ratio of the total amount of ions recorded by the ion collectors to the total amount of atoms ejected from the crater volume, was estimated to be about 0.25% at FP≈0.

Summary

The dependence of the total charge carried by ions recorded by the ion collector on the laser beam focus position FP correlates qualitatively with the dependence of the ablation efficiency on FP, calculated from the crater volume measurements. The total amount of plasma ions is, however, only a small part (~0.25%) of the total amount of atoms ejected from the crater.

At sharp focusing the laser beam on the target (FP=0) the crater diameter is much larger (crater diameter/laser beam spot size ≈7) than the theoretical diameter of the beam waist. At strong defocusing the laser beam the crater diameter is close to the diameter of the beam.

The large crater volume and the hemispherical shape (crater diameter/crater depth ≈1.8) can be best explained by shock-wave cratering process. It is believed, that large-area damages surrounding the crater results from melting of the target surface by far-field diffraction pattern of the focused laser beam, lateral heat transport and/or by heating the surface by X-rays emitted from the plasma.

Acknowledgments We are grateful to Mrs. H. Włodarczyk and Mrs. J. Pokorska for performing the replicas of craters and for the optical microscopy investigations of the target craters and their replicas. The work was supported by the EC for projects PALS/005 and

PALS/006, and the IAEA, Vienna, financial support (contract no. 11535/RD).

References

1. Anisimov SI, Prokhorov AM, Fortov VE (1984) Primenenie moshchnykh lazerov dla issledovania veshchestva pri sverkhvysokikh davleniakh. Uspekhy Fizicheskikh Nauk 142:395–434
2. Burton WM (1983) Cometary particle impact simulation using pulsed lasers. In: Advances in space research: Symposium on Impact Processes. Proc COSPAR. Ottawa 2;12:61–64
3. Burton WM, Wallis MK (1982) The analogy between pulsed laser irradiation and hypervelocity dust particle impacts. In: Proc Int Conf on Cometary Exploration. Budapest 3:215–222
4. Busquet M (1982) Mixed model: Non-local-thermodynamic equilibrium, non-coronal-equilibrium simple ionization model for laser-created plasmas. Phys Rev 25:2302–2323
5. Eidmann K, Amiranoff F, Fedosejevs R *et al.* (1984) Interaction of 1.3-μm laser radiate with thin foil targets. Phys Rev A 30;5:2568–2589
6. Hauser T, Scheid W (1991) Energy and angular distribution of ions emitted from a plasma after relativistic self-focusing of laser beams. Laser Part Beams 9;3:675–690
7. Jungwirth K, Cejnarova A, Juha L *et al.* (2001) The Prague Asterix laser system. Phys Plasmas 8;5:2495–2501
8. Nowak-Goroszczenko A, Mróz W, Wołowski J, Woryna E (1992) Strongly coupled plasma in laser-target experiments. In: Ebeling W *et al*. (eds) Physics of nonideal plasmas. BG Teubner-texte zur Physik, Band 26. Stuttgart-Leipzig, pp 303–310
9. Obenschain SP, Grun J, Ripin BH, McLean EA (1981) Uniformity of laser-driven, ablatively accelerated targets. Phys Rev Lett 46;21:1402–1405
10. Pirri AN (1977) Theory for laser simulation of hypervelocity impact. Phys Fluids 20;2:221–228
11. Ready JF (1971) Effect of high-power laser radiation. Academic Press, New York-London
12. Willmott PR, Huber JR (2000) Pulsed laser vaporization and deposition. Rev Modern Phys 72;1:315–329
13. Woryna E, Parys P, Wołowski J, Mróz W (1996) Corpuscular diagnostics and processing methods applied in investigations of laser-produced plasma as a source of highly ionized ions. Laser Part Beams 14;3:293–321
14. Ye M, Grigoropoulos CP (2001) Time-of-flight and emission spectroscopy study of femtosecond laser ablation of titanium. J Appl Phys 89;9:5183–5190
15. Yoo JH, Jeong SH, Greif R, Russo RE (2000) Explosive change in crater properties during high power nanosecond laser ablation of silicon. J Appl Phys 88;3:1638–1649
16. Zhigilei LV, Garrison BJ (2000) Microscopic mechanisms of laser ablation of organic solids in the thermal and stress confinement irradiation regimes. J Appl Phys 88;3:1281–1298